



Heteropoly Acid Functionalized Fluoroelastomer with Outstanding Chemical Durability and Performance for Vehicular Fuel Cells

Journal:	<i>Energy & Environmental Science</i>
Manuscript ID	EE-ART-02-2018-000545.R1
Article Type:	Paper
Date Submitted by the Author:	21-Mar-2018
Complete List of Authors:	<p>Motz, Andrew; Colorado School of Mines, Department of Chemical and Biological Engineering Kuo, Mei-Chen; Colorado School of Mines, Department of Chemical and Biological Engineering Horan, James; Colorado School of Mines, Department of Chemical and Biological Engineering Yadav, Rameshwar; Nissan Technical Center Inc Seifert, Sönke; Argonne National Laboratory, X-ray Science Division Pandey, Tara; Colorado School of Mines, Chemical and Biological Engineering Galioto, Samuel; Colorado School of Mines, Department of Chemical and Biological Engineering Yang, Yuan; Colorado School of Mines, Chemistry Dale, Nilesh; Fuel Cell and Battery Laboratory, Zero Emission – Research Nissan Technical Center North America Hamrock, Steven; 3M Company, Herring, Andrew; Colorado School of Mines, Department of Chemical and Biological Engineering</p>



Journal Name

ARTICLE

Heteropoly Acid Functionalized Fluoroelastomer with Outstanding Chemical Durability and Performance for Vehicular Fuel Cells

Andrew R. Motz,^a Mei-Chen Kuo,^a James L. Horan,^a Rameshwar Yadav,^b Soenke Seifert,^c Tara P. Pandey,^a Samuel Galioto,^a Yuan Yang,^d Nilesh V. Dale,^b Steven J. Hamrock,^e and Andrew M. Herring,^{a*}

Received 00th January 20xx,
Accepted 00th January 20xx

DOI: 10.1039/x0xx00000x

www.rsc.org/

To further facilitate commercialization of automotive fuel cells, durability concerns need to be addressed. Currently the addition of a mechanical support in the membrane is able to adequately solve issues of mechanical degradation, but chemical degradation *via* oxygenated radical attack remains an unsolved challenge. Typical mitigation strategies use cerium or manganese species to serve as radical scavengers, but these ions are able to migrate in the membrane and even leach out of the system. The approach used in this study is to covalently link and immobilize a heteropoly acid (HPA), more specifically 11-silicotungstic acid (HSiW11), a lacunary HPA of the Keggin structure to a fluoroelastomer, serving as both a radical decomposition catalyst and the proton conducting acid. This dual functionality allows for both high content of radical scavenging species and high ion exchange capacity. An efficient three step, high yield (77%), commercially viable synthesis for this polymer is reported. The synthesis route for making this new heteropoly acid functionalized polymer is confirmed using infrared (IR), nuclear magnetic resonance (NMR) spectroscopy, and thermogravimetric analysis (TGA). The material exhibits clustering of the HSiW11 moieties, resulting in a poorly connected proton conducting phase when dry, but excellent conductivity is achieved at elevated humidities (0.298 S cm⁻¹ at 80°C and 95 %RH). The proton conductivity shows an enhancement above 60 °C due to a softening of the polymer, as shown by DSC. Under an aggressive chemical accelerated stress test (AST), 90 °C, 30 %RH, zero current, and pure O₂, the PolyHPA losses only 0.05 V of open circuit voltage (OCV) after 500 h, greatly out performing any other material reported in literature. For comparison, the Nafion® N211 fuel cell drops below 0.8 V after only 76 h under the same conditions. In fuel cell testing the PolyHPAs have outstanding chemical stability and also possess very low *in-situ* high frequency resistance (HFR) leading to high performance (1.14 W cm⁻² at 2 A cm⁻²), compared to 1.11 W cm⁻² for the Nafion® N211 fuel cell at the same current. At 75 wt% HSiW11 loading, the fuel cell HFR showed a 22% decrease over N211.

Broader Context

Fuel cell electric vehicles (FCEV) are already on the market and many more are expected to be released in the next few years. For transportation, FCEVs have several inherent advantages over battery electric vehicles, such as rapid refuelling (<5 min) and decoupled energy density / power density. Also, cost does not scale linearly with respect to vehicle range, creating an advantage for FCEVs in markets where longer range is desired. The fuel, hydrogen, stores energy in the form of chemical bonds and when oxidized produces water, providing one promising avenue for increased sustainability, decreased carbon emissions, and decreased pollution at the point of use, providing hydrogen comes from renewable resources. Hydrogen is currently produced from natural gas (the most cost effective source), but water electrolysis is rapidly coming down in price. Water electrolysis will, when coupled with renewable electricity generation, such as wind or solar, provides fully renewable and sustainable hydrogen. While the technology is already advanced enough to commercialize, reducing overall cost, improving durability, and increasing hydrogen availability are still needed for mass adoption of FCEVs. A major current challenge is achieving adequate chemical and mechanical membrane durability while also maintaining or even enhancing fuel cell performance.

^a Department of Chemical and Biological Engineering, Colorado School of Mines, Golden, Colorado 80401, USA. E-mail: aherring@mines.edu

^b Nissan Technical Center North America, Farmington Hills, Michigan 48331, USA

^c X-ray Science Division, Advanced Photon Source, Argonne National Laboratory, Argonne, IL 60439, USA

^d Department of Chemistry and Geochemistry, Colorado School of Mines, Golden, Colorado 80401, USA

^e Energy Components Program, 3M, St. Paul, MN 55144, USA

† Footnotes relating to the title and/or authors should appear here.

Electronic Supplementary Information (ESI) available: [details of any supplementary information available should be included here]. See DOI: 10.1039/x0xx00000x



Journal Name

ARTICLE

Introduction

Fuel cells are electrochemical energy conversion devices, which can directly convert the energy stored in chemical bonds into electricity. The volumetric and gravimetric power and energy density of polymer electrolyte fuel cells are such that they represent a promising replacement to the internal combustion engine for automotive applications. Major improvements in fuel cell design have been made to simplify the overall system through adoption of thinner membranes, which allow for back diffusion of water and improved performance with dry inlet gasses.^{1, 2} Additional work to reduce catalyst loading has been successful, resulting in the projected stack cost dropping below \$15 per kW when mass produced.³ These advances have enabled the beginning of commercialization of fuel cell electric vehicles (FCEV). Improved platinum utilization and increased power density would reduce fuel cell stack size and materials cost, further reducing the barriers to fuel cell technology. In addition to reducing the initial cost, durability should be improved. Polymer electrolyte membranes undergo two main types of degradation, chemical and mechanical, and the two degradation pathways have been proposed to have a synergistic effect on each other.^{4, 5, 6, 7} For longevity in real world devices, it is thus imperative to have both outstanding chemical and mechanical durability. Adding mechanical support to the membrane is able to satisfy the need for mechanical durability through decreasing swelling and improving strength, but chemical degradation mitigation techniques are still not satisfactory for the needs of a fuel cell system.^{8, 9}

Polymer electrolyte membranes need to have good ion-transport, high electrical resistance, and provide a good barrier to reactant gasses for good performance and also need to be durable under conditions in which a real device will experience. Many new materials have been synthesized and studied, but none have been able to simultaneously meet all of the aforementioned criteria and provide enough benefit over the perfluoro sulfonic acids (PFSA) for wide adoption.^{10, 11, 12, 13} One potential factor is the reliance on the pendent sulfonic acid groups in a majority of these materials which require high water content, high concentration of protons, or both to result in ionic conductivity over 0.1 S cm^{-1} . One notable advance in hydrocarbon membranes is the use of a coating containing nanocracks, which are able to act at a barrier to loss of water at elevated temperatures, and thus retain high proton conductivity under low humidity conditions.¹⁴ A large number

of these materials are hydrocarbon based and chemical stability data is not available.

A Preliminary effort to improve the chemical stability of the PFSA polymers was to treat the polymer with elemental fluorine to minimize the number of reactive carboxylic acid end groups, but once main chain scission occurs this method becomes ineffective.^{15, 16} Second generation efforts to improve the chemical stability of the PFSA materials were to add some radical decomposition catalyst, most notably CeO_2 or MnO_2 .^{17, 18, 9} These additives can be introduced as a composite material or the Ce^{3+} and Mn^{2+} ions can partially neutralize the H^+ ions, effectively lowering the number of protons available for transport and therein reducing the cell performance. There is a trade-off where durability is greatly improved, but the performance is not greatly decreased, unfortunately, the Ce^{3+} and Mn^{2+} ions are still free to move in the electrolyte domain and accumulation of them in the cathode catalyst layer is cause for concern.^{19, 20, 21} More recently a composite approach has been demonstrated using zirconia doped ceria additives which show further reduction of open circuit voltage loss.²²

An alternative class of additives that have shown promise in mitigating chemical degradation are heteropoly acids (HPAs), a sub-class of the polyoxometalates.^{23, 24, 25, 26} HPAs are a large class of super acids, which also may serve as radical decomposition catalysts. It is important to note here that phosphotungstic acid ($\text{H}_3\text{PW}_{12}\text{O}_{40}$) will decompose in the presence of radicals forming the Ishii-Venturello catalyst, whereas silicotungstic acid ($\text{H}_4\text{SiW}_{12}\text{O}_{40}$) is known to be stable under similar conditions.^{27, 28, 29} Phosphotungstic acid and its caesium salt have shown the ability to improve both the proton transport and chemical stability of sulfonated poly(ether ether ketone) (sPEEK), but using this approach has not yet been proven to result in performance and stability parity with Nafion® N211.^{30, 31} Past efforts to incorporate HPAs into membranes have been hindered due to the HPA migration, clustering, or leaching out due to their high solubility in water.^{32, 33} One potential solution to this challenge that has recently been investigated is encapsulating the HPA in carbon nanotubes.^{34, 35} In addition to the antioxidant properties of HPAs, they are also known to be very proton conductive even with limited hydration.^{36, 37} By acting as an ion conducting moiety and a radical scavenger, a win-win situation occurs where more HPA can theoretically increase the H^+ transport and increase the chemical stability, bypassing the trade-offs associated with Ce and Mn doping. More recently our group has demonstrated a material with covalently immobilized 11-silicotungstic acid (HSiW11) as the only ion-conducting group, resulting in a shift in the paradigm from previous HPA containing membranes.^{38, 39}

Herein, we report a three-step, highly efficient synthesis producing a membrane achieving the chemical durability breakthrough the community has been searching for. Using a novel ion-conducting material that contains HSiW11 hybrid moieties covalently bound to a commercial fluoroelastomer, resulted in a thin, conductive, and chemically robust membrane. We have demonstrated that this material has lower, *in-situ* transport resistance and vastly greater chemical stability than the state of the art polymer electrolyte.

Experimental

Materials

Diethyl (4-hydroxyphenyl)phosphonate (DHPP) was purchased from Synquest (catalog number 6677-1-07) and a polyvinylidene-co-hexafluoropropylene (PVDF-HFP) fluoroelastomer (FC-2178) was supplied by 3M. Hydrochloric acid (HCl) (37%, ACS reagent grade) was purchased from Pharmco-Aaper. Sodium hydride (NaH) (60% dispersion in oil) and bromotrimethylsilane (TMSBr) (97%) were purchased from Sigma-Aldrich. All other reagents were purchased from Sigma-Aldrich with >99% purity and were used as received.

Preparation of PolyPPE

FC-2178 (31.78 g) was washed with methanol, dried at 40 °C under vacuum for two days, then dissolved in 150 mL anhydrous dimethylformamide (DMF). In a separate flask, 20.0 g DHPP was added to 100 mL anhydrous DMF and allowed to dissolve at room temperature, followed by cooling to 0 °C. Once cooled, NaH was added slowly to the DHPP solution, under a N_{2(g)} flow, producing H_{2(g)} bubbles. After 2 h, bubble formation subsided and the FC-2178 solution was slowly added over a period of 30 minutes. The combined solution was then heated to 50 °C and allowed to react for 24 h, darkening with time, before precipitation in 1M HCl. The precipitate is then isolated, washed with water, and dried under vacuum for 48 h, producing phenol phosphonic ester functionalized FC-2178 (PolyPPE).

Preparation of PolyPPA

The PolyPPE was then dissolved in 450 mL acetonitrile overnight at room temperature. The following day, 32 mL bromotrimethylsilane (TMSBr) was added under a N₂ environment. The reaction was heated to 45 °C and allowed to react overnight, producing a cloudy mixture. The reaction solution was filtered and the filtrate was dissolved in 600 mL MeOH with 20 mL concentrated HCl, quenching the reaction. The reaction solution was dried resulting in the phenol phosphonic acid functionalized FC-2178 (PolyPPA). The PolyPPA was subsequently washed with water, dried, and stored at room temperature, yield = 38.5g (77%).

Preparation of PolyHPA

4.50 g PolyPPA was added to 180 mL n,n- dimethylacetamide (DMAc) and allowed to dissolve overnight at 80 °C. Next, 10.50

g α -K₈SiW₁₁O₃₉•13(H₂O) (HSiW11), synthesized according to the protocol previously reported,²⁷ was slowly added. The mixture was cloudy, but rapid stirring with a magnetic stir bar ensured no precipitate formed on the bottom. Next, 12 M HCl (1.356 mL) was added dropwise, turning the solution into a transparent amber. The reaction took place over 70 h at 80 °C, then the solution was filtered with a paper filter followed by a filtration using a medium porosity glass frit Büchner Funnel to remove potassium chloride crystals. The volume was then reduced to ca. 60 mL using a rotary evaporator. This solution was then cast on Kapton® using a doctor blade to control thickness and dried at room temperature over night (16 h). When dried, the films ranged from 20-80 μm. Next, thermal annealing under pressure (5 min, 26.7 kN, 160 °C) was used to finish the attachment reaction and make the film more uniform. The resulting film was then soaked in 1 M H₂SO₄ to ion-exchange (3x) followed by rinsing in DI water (3x). Each rinse was more than 1 h.

Materials Characterization

Fourier Transform Infrared Spectroscopy (FT-IR). FT-IR was collected using a Nicolet Nexus 470 FT-IR E.S.P equipped with a Specac Golden Gate attenuated total reflection (ATR) stage at ambient conditions. All spectra were collected with 512 scans and a resolution of 1 cm⁻¹. All polymers were measured in the membrane form and the small molecules were measured as powders.

Nuclear Magnetic Resonance Spectroscopy (NMR). Liquid NMR spectra were recorded on a Joel ECA 500 MHz spectrometer in DMSO-d₆ solvent. The chemical shifts for ¹H, ¹⁹F, ³¹P were based on tetramethylsilane, trichlorofluoromethane, and phosphoric acid standards, respectively. The solid state ¹H → ³¹P CP/MAS measurements were performed on a 400 MHz Bruker spectrometer using triphenylphosphine (-6ppm) as a standard.

Thermogravimetric Analysis (TGA). TGA experiments were performed using a TA instruments TGA Q 500 using a platinum pan. The ramp rate was 5 °C per minute up to 800 °C with a gas flow rate of 40 mL min⁻¹. Samples were dried at 80 °C for 1 h followed by equilibration at ambient conditions for an additional hour. Experiments were run using N₂ or air.

Differential Scanning Calorimetry (DSC). The DSC data was collected on a TA instruments DCS Q20 in TZero aluminum pans with hermetic lids. The heating scan rate was 10 °C min⁻¹ and the cooling rate was 40 °C min⁻¹. Two cycles from -30 to 130 °C were first conducted, followed by two cycles up to 200 °C.

Potentiostatic Electrochemical Impedance Spectroscopy (PEIS). PEIS experiments were performed in a TestEquity environmental chamber to accurately control the temperature

and relative humidity. The membranes were placed across four platinum electrodes in cells designed after Bekktek FC-BT-115 conductivity cells and the PEIS measurements were performed using a BioLogic VMP3 potentiostat. Data were fit using a Randles circuit and the results were used to calculate an in-plane conductivity.

Focused Ion-Beam (FIB) milling and Transmission Electron Microscopy (TEM). The sample was milled with Gallium ions using a Helios NanoLab 600i focused ion beam and placed on a TEM grid. The transmission electron microscopy (TEM) was performed using a FEI TalosF200X.

Small Angle X-ray Scattering (SAXS). The SAXS data was collected on beamline 12-ID-B at the Advanced Photon Source, Argonne National Lab in a custom built environmental chamber, using 13.3 keV radiation. The chamber, described in detail elsewhere,⁴⁰ is able to control temperature and humidity and the conditions are outlined below. A Pilatus 3M detector was used.

Environmental Scanning Electron Microscopy (ESEM) and Energy Dispersive Spectroscopy (EDS). The electron scanning microscope used was a FEI Quanta 600 operating under low vacuum. All SEM images shown were taken with a solid-state backscatter electron detector. The EDS was performed with an element EDAX at 20 keV. Standard parameters were used to quantify elements using EDAX Genesis software.

Fuel Cell Testing. The Nafion[®] standard membrane electrode assembly (MEA) was fabricated using a catalyst coated membrane (CCM), Nafion[®] N211, with catalyst supplied by Tanaka Holdings Co. Ltd. The anode catalyst layer consisted of TEC10EA30E, 30% Pt/C, 0.055 mg cm⁻² and a cathode catalyst layer consisted of TEC10E50EHT, 50% Pt/C, 0.35 mg cm⁻² and had an active area of 2x5 cm². The PolyHPA MEAs were fabricated using commercial gas diffusion electrodes (GDE)s for both the anode and cathode (Johnson Matthey Pt/C electrocatalyst, PFSA ionomer, 0.35 Pt mg cm⁻²). The PolyHPA-70 (70 wt% theoretical HSiW11 loading) MEA had an active area of 2x5 cm² and the PolyHPA-75 (75 wt% theoretical HSiW11 loading) MEA was 5 cm². The 10 cm² fuel cells were run using flow rates, 4 L min⁻¹ at the anode and 8 L min⁻¹ at the cathode while the 5 cm² fuel cell was run using flow rates of 2 L min⁻¹ at the anode and 4 L min⁻¹ at the cathode.

Accelerated Stress Testing (AST). The mechanical AST was performed on an MEA in standard fuel cell hardware at 80 °C with N₂ flow on both the anode and cathode and the humidity of each was switched from 100 %RH to 0 %RH holding for 30s on each, making a 1 min cycle. The test was stopped and hydrogen crossover was tested using linear sweep voltammetry with a scan rate of 1 mV s⁻¹, after 5750, 10000 and 22500 cycles. The chemical ASTs were performed on an

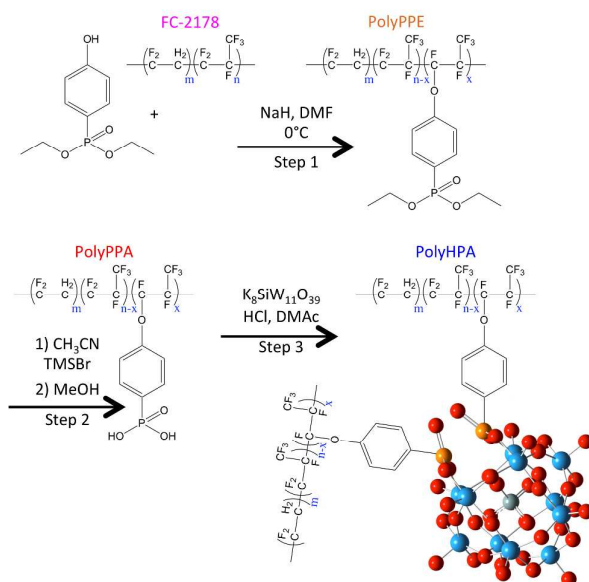
MEA in standard fuel cell hardware by holding the fuel cell at open circuit voltage (OCV), 90°C, 30%RH anode and cathode, zero current, and H₂/O₂ flow.

Results and Discussion

Synthesis

A four-step synthesis, reported elsewhere,⁴¹ was used to covalently attach HSiW11 to FC-2178, where hexafluoropropylene accounts for ca. 20 mol% of the polymer.⁴² This original synthesis method involved attachment of diethyl (4-hydroxyphenyl)phosphonate (DHPP) sidechains to FC-2178 utilizing K₂CO₃ as a reactant. The K₂CO₃ can ion-exchange with the alcohol to form an alkoxide (-O⁻K⁺) and potassium bicarbonate (KHCO₃). Both alkoxide and K₂CO₃ are then able to dehydrofluorinate the FC-2178, creating unsaturated bonds, and enabling attachment of the alkoxide. Because K₂CO₃ is a poor nucleophile, it will not attach to the polymer and only the alkoxide will become covalently attached. This chemistry is based on methods that have been used to cross-link PVDF-HFP.^{43, 44} The reaction resulted in excessive unsaturated bonds remaining in the final product and the films had extremely poor mechanical properties.

To avoid the over dehydrofluorination, the reagent was changed to NaH, as the hydride is a stronger base than K₂CO₃, but still a weak nucleophile. This change allows for attachment of DHPP at much lower temperatures. The resulting phenol phosphonic acid functionalized FC-2178 (PolyPPA, see Scheme 1), a transparent yellow film, was much lighter in color than the PolyPPA made using K₂CO₃, which was almost black. The work described here was done using the much stronger PolyPPA produced *via* the process outlined in Scheme 1.



Scheme 1: Full synthetic reaction scheme for the synthesis of PolyHPA (final product) from FC-2178 and DHPP

The method for functionalizing lacunary heteropoly acids with small organic molecules has been well documented,^{45, 46} but this work involves attaching HSiW11 to a preformed engineering polymer chosen for its strength and stability. Attachment of HSiW11 to a preformed polymer, to the authors knowledge, has not been previously reported in the peer-reviewed literature.

The final product is referred to as PolyHPA-x where x indicates the mass fraction of α -K₈SiW₁₁O₃₉•13(H₂O) (HSiW11), added to the reaction (Scheme 1, step 3), with the remaining mass consisting of PolyPPA. A majority of the studies were done on PolyHPA-70 and some data exist for the higher loading material, PolyHPA-75. Unfortunately at 75 wt% loading the mechanics of the film resulted in challenges for more comprehensive fuel cell testing, but what was achieved, see below, shows much potential for the future use of these films. For the fuel cell testing of the PolyHPA-75 material, a 10 cm² MEA could not be fabricated and the active area was 5 cm². All films were thoroughly washed in acid followed by water at room temperature showing that the HSiW11 moiety was indeed covalently attached. IR and NMR characterization and discussion is available in the supplementary information (SI).

Membrane Characterization (Ex-situ Evaluation)

The thermal stability was investigated with TGA on the PolyPPA and PolyHPA-70, see data in Figure S3. The PolyPPA has several distinct decomposition regions. First, marginal weight loss occurs before 280 °C, all of which has been assigned to loss of water and has been previously observed in HPA containing materials.^{47, 48} Next, between 280 and 400°C there is a constant and substantial loss at 0.2% per °C. Finally, two inflection points exist at 420°C and 490°C where the latter only exists in the presence of air, a more oxidizing environment. PVDF-HFP has a thermal decomposition temperature near 450°C in N₂,^{49, 42} but no significant mass loss occurs beforehand. This indicates that the decomposition event starting at 280 °C is likely due to the decomposition or loss of the sidechain. Data and more in depth discussion are available in the SI (**Error! Reference source not found.**).

HPAs can undergo a loss of two H⁺ and a terminal oxygen to form water, thereby reducing the concentration of mobile H⁺ in the film. This decomposition is difficult to discern from loss of bound water and theoretically has a strong variance on partial pressure of water.⁵⁰ With the high decomposition temperature of this material, it is mostly limited by loss of charge (not seen in TGA). In an oxidizing environment, HSiW11 moieties are known to decompose into WO₃ and SiO₂, the most oxidized forms of W and Si.⁴⁸

HPAs are known to be unstable in alkaline conditions and therefore traditional titrations to measure ion-exchange capacity (IEC) are not possible and therefore the WO₃ and SiO₂ residue mass was used to calculate the IEC. This calculation, available in the SI, suggests that a large portion of water stable inorganic material has been added to the polymer. The residue at 800 °C in air is ca. 4 % and 55 % for the PolyPPA and PolyHPA-70, respectively. The resulting IEC of 0.86 mmol H⁺/g

PolyHPA-70 indicates that nearly all of the added HSiW11 is stable to soaking in acid followed by water at room temperature, for more details, please see the SI. These films are stable to acidic and aqueous environments at room temperature and humidified air at elevated temperatures, but when the films are soaked in warm water (80 °C) some of the HSiW11 leaches out.

The DSC data can be seen in Figure S4 and has two clear transitions. First, at 60°C there is a thermal transition in both the PolyPPA and PolyHPA-70. The T_α for PVDF-HFP with a similar monomer ratio is -13 °C and so we assign this new transition to the T_β of the sidechains.⁵¹ According to the ³¹P NMR data, some of the phenol phosphonic acid sidechains still exist in the final PolyHPA-70 film and therefore the T_β is still observed. In the first heating of the PolyHPA-70 (non-annealed) there is an endothermic transition starting near 160°C which could be a chemical reaction or crystallization. An *in-situ* SAXS annealing experiment was performed on PolyHPA-70 (non-annealed) to observe the morphological changes when annealed, but no indication of change in the morphology was observed, (see **Error! Reference source not found.**). Using this knowledge, all films were processed at 160°C for 5 min to enhance crosslinking and avoid thermal decomposition.

The proton conductivity, seen in Figure 1, is >0.1 S cm⁻¹ at all of the temperatures measured (50-90 °C and 95 %RH) and exhibits two different regimes of transport that intersect near 60 °C, the T_β of the hydrophilic sidechains. The values at 80 °C and 95 %RH are remarkably high, 0.228 and 0.298 S cm⁻¹ for the PolyHPA-70 and PolyHPA-75, respectively. This high conductivity is achieved due the super acidic, and thus highly mobile, nature of the protons of silicotungstic acid. At lower temperatures, the energy barrier for transport is over 4 times greater than when compared to above 60 °C (ca. 8 kJ mol⁻¹). This is much lower than the activation energy for Nafion[®] under similar conditions, which has been reported to be 12.5 kJ mol⁻¹.⁵² This conductivity should enable high performance, practical devices and contributes to the low *in-situ* area specific resistances, discussed below.

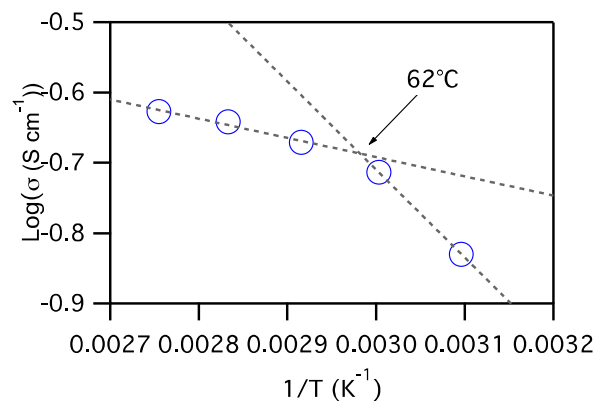


Figure 1: In-plane conductivity of PolyHPA-70 at 95%RH and various temperatures with trend lines to guide the eye

The polymer's morphology was investigated using FIB / TEM under vacuum and SAXS under conditions relevant to fuel cell operation (elevated temperature and humidity). We first consider the SAXS equilibrated in air. The SAXS data was recorded using hard synchrotron x-rays and is dominated by contributions from heavy elements, *i.e.* W. Two peaks appear in the SAXS, one at 0.097 \AA^{-1} and another at 0.6 \AA^{-1} corresponding to d-spacing values of 6.5 and 1.0 nm (Figure 2a). The 1.0 nm feature is likely the spacing between two adjacent HSiW11 molecules and the 6.5 nm feature is likely the spacing between HSiW11 rich and deficient domains. The underlying Porod slope is *ca.* -4, indicating that all features are likely spherical. Examination of the high q peak, Figure 2b, shows a shift to lower q, or larger d-spacing that is highly dependent on RH. This is indicative of water moving towards the surface of the HSiW11 moieties and pushing them further apart. The peak at 6.5 nm is nearly unchanged with humidity, indicating that additional water is not affecting this feature. Interestingly with this system of HSiW11 and PolyPPA, this

same SAXS pattern always occurs after the material is processed. This strongly implies that a thermodynamic minimum, with the processed film, is achieved with clusters of HSiW11 separated by a characteristic length of *ca.* 6.5 nm. Looking at the TEM (Figure 2c) it appears as if two levels of clustering exist. Bright spots in the TEM backscattered micrograph indicate regions with more heavy elements and from the EDS measurements (**Error! Reference source not found.**), it is clear that the heaviest element in high concentration is W, therefore the bright spots must represent a phases enriched in W. First, there are three large clusters, which are at an irregular distance from each other, and therefore no d-spacing is observed in the SAXS data. On further investigation, many 3-4 nm clusters appear which are separated by a darker phase. The center to center distance of these smaller clusters is assigned to the 6.5 nm peak seen in the SAXS data. A drastic change is noted in the scattering pattern of the liquid soaked film, Figure 2a.

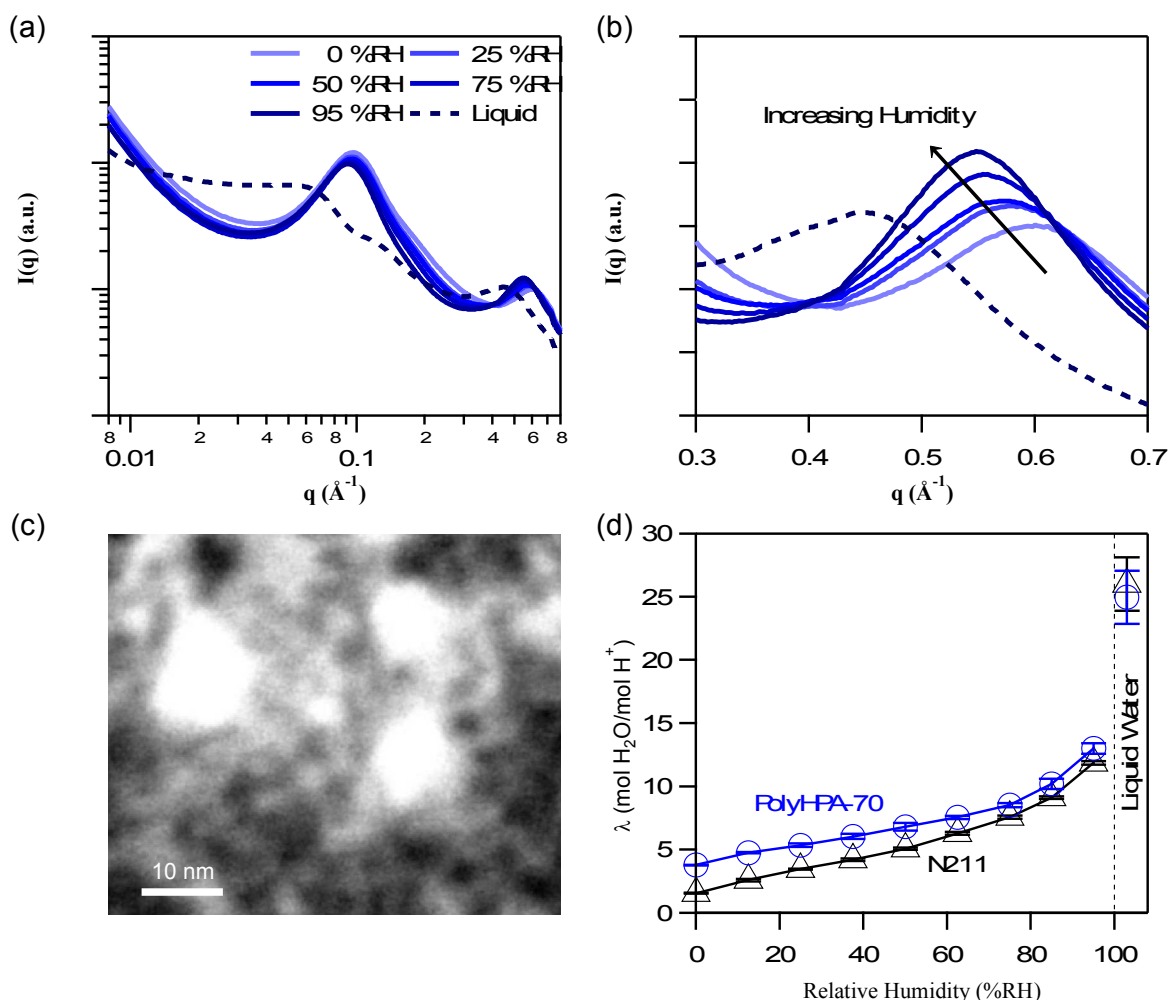


Figure 2: (a) SAXS at 80°C in air at various humidities and in liquid water (b) High q region of the SAXS (c) TEM darkfield micrograph of PolyHPA-70 that was milled out from the bulk of the film using FIB (d) λ vs. relative humidity for Nafion[®] (Δ) and PolyHPA-70 (\circ) at 60°C



Journal Name

ARTICLE

This change is likely a change from scattering dominated by structure factor scattering (as indicated by peaks) to a spectra dominated by form factor scattering (lower intensity and dominated by shoulders), as indicated by the loss in peaks and drop in intensity.^{53, 54, 55} We are now able to observe several radii of gyration (R_g) with values of 10, 4.2, and 1.3 nm. The feature with an R_g of 10 nm is assigned to the large bright clusters in Figure 2c while the feature with an R_g of 4.2 nm is assigned to the clusters that are separated by 6.5 nm. Lastly, the feature with a 1.3 nm R_g is assigned to the individual, solvated HSiW11 moieties.

It is hypothesized that increasing the continuity of the HSiW11 phase could serve to further improve the transport properties of the PolyHPA material, which would make this material a better proton conductor under hotter and drier conditions. As compared to the Nafion[®] standard the water content in the film, more water per protogenic group is present at all humidities (See Figure 2d). The difference is most dramatic at low humidities where the highly hydroscopic nature of the HSiW11 causes retention of 3.79 H_2O/H^+ (15.1 per HSiW) in dry N_2 at 60 °C, as determined by TGA, compared to 1.55 for Nafion[®].⁵⁶ In liquid water the PolyHPA-70 has a similar λ as Nafion[®], but its swelling behaviour is different. The dimensional swelling of Nafion[®] N211 was measured at $\Delta_z = 2 \pm 2\%$ and $\Delta_{x-y} = 32 \pm 7\%$ in contrast, the PolyHPA-70 film dimensional swelling was $\Delta_z = 24 \pm 5\%$ and $\Delta_{x-y} = 56 \pm 5\%$.

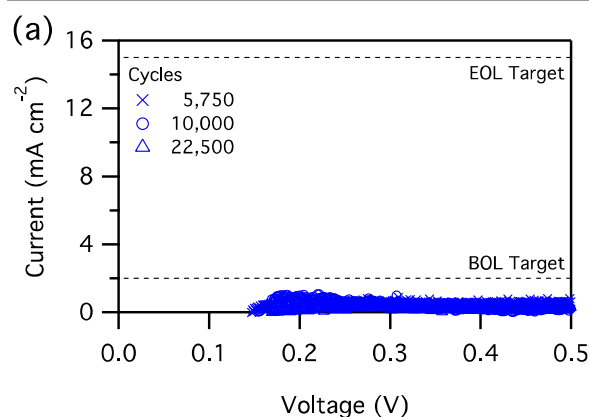
As the film is humidified and the water content increases, the 1 nm peak shifts to lower q and thus higher d -spacing. This is not true for the 6.5 nm peak and is an indication that more water is not hydrating the HSiW11 in the 6.5 nm peak until the film is immersed in liquid water.

Chemical and Mechanical Stability

This material has been designed to solve the chemical stability issues discussed in the introduction through incorporation of a large amount of HSiW11 (a radical decomposition catalyst) into a polymer film. To probe the chemical and mechanical stability of these materials, accelerated stress tests (ASTs), based on U.S. Department of Energy (DOE) suggested protocols, were performed.^{57, 58, 59} Several PolyHPA-70 (80 μm) films were used for preliminary testing. The first film easily passed the mechanical AST with $<1 \text{ mA cm}^{-2}$ hydrogen crossover after 22,500 wet dry cycles (LSV can be seen in Figure 3a) which has been previously reported.⁴¹ This particular MEA was fabricated using a CCM and the fuel cell performance was rather poor given the high proton conductivity. The end of life fuel cell performance is shown in **Error! Reference source not found.** The rest of the fuel cells were fabricated using commercial GDEs, which resulted in

much greater performance, see below. While this is an achievement, films with mechanical support are often able to easily pass this AST and this problem is considered solved by many in the community. The challenge that motivated this research was making a film that was highly chemically stable. To test the hypothetical chemical stability of this material, a chemical AST was performed at 90 °C, 30 %RH, under an H_2 - O_2 environment at OCV. Under these conditions, standard polymer electrolyte membranes degrade rapidly, this is due to radical generation and subsequent attack by the radicals of the polymer film. It has been previously demonstrated that the decay is much more rapid under an O_2 environment, as used here, as opposed to air, the standard DOE protocol.⁶⁰ Under O_2 during this test Pt has been shown to dissolve and precipitate as a Pt band in the membrane, this phenomenon is also seen in real fuel cells that are cycled through OCV. The accelerated degradation, in the AST using O_2 , has been attributed to decomposition of the PFSA polymer near the Pt band, which is more prevalent in O_2 environments.⁶¹ Below in Figure 3b is the OCV vs. time for two different batches of PolyHPA-70 (80 μm) and a Nafion[®] 211 control.

This remarkably low OCV decay (100 $\mu V \text{ h}^{-1}$), without OCV recovery, and under very harsh conditions represents the lowest rate reported to date in the literature.⁶² This accomplishment is particularly remarkable because the HSiW11 acts as both the proton conducting moiety and the radical decomposition catalyst allowing for high performance with a highly chemically and mechanically stable material.



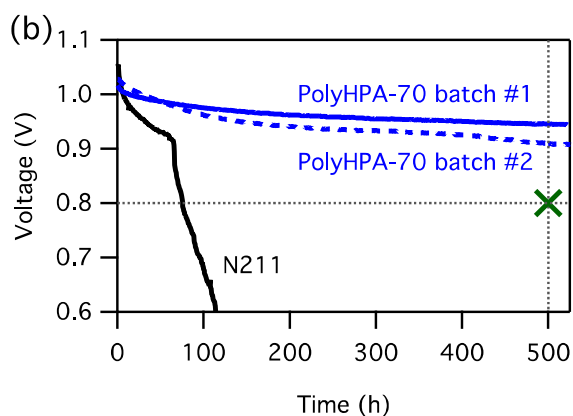


Figure 3: (a) LSV for PolyHPA-70 (80 μm) after wet/dry cycling and beginning of life and end of life crossover targets (b) OCV hold test at 90 $^{\circ}\text{C}$ / 30 %RH under $\text{H}_2\text{-O}_2$ flow and no current. Two different batches of PolyHPA-70 (80 μm) easily pass the test while Nafion[®] N211 film for comparison (bottom trace). The typical target is 500 h while retaining a voltage above 0.8 V which is marked (x)

Fuel Cell Performance (*In-situ* Evaluation)

In addition to the chemical stability, this material was designed to have exceptional H^+ transport properties, as HPAs are some of the most conductive solids known due to their highly delocalized negative charge, as stated in the introduction. A 48 μm film of PolyHPA-70 and a 20 μm film of PolyHPA-75 were used to fabricate fuel cells where the films had 70 and 75 theoretical wt% HSiW11 loadings, respectively. The performance under an $\text{H}_2\text{-O}_2$ or an $\text{H}_2\text{-air}$ environment were evaluated, and compared with an MEA constructed from Nafion[®] N211 and standard electrodes optimized for Nafion[®] N211. The PolyHPA fuel cells do not utilize optimized electrodes and the testing presented here is used solely to evaluate the PolyHPA membranes and are not to be taken as the performance of a future optimized fuel cell, using these materials. In fact, this is evident from the mass transfer limitations observed under $\text{H}_2\text{-air}$ operation.

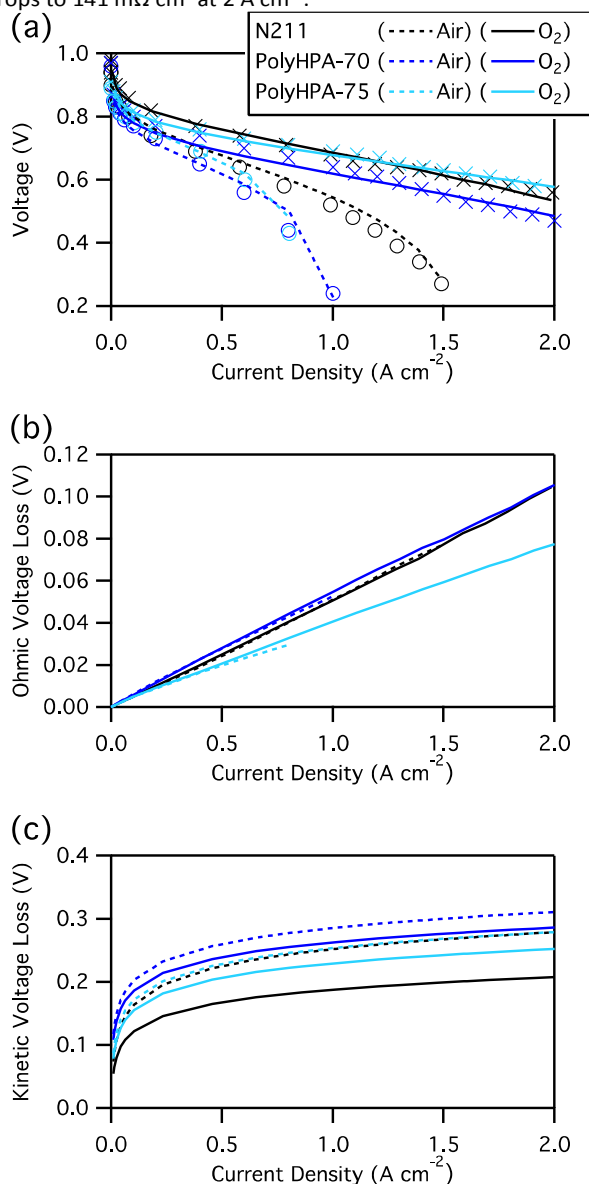
The I-V performance of the PolyHPA-75, PolyHPA-70 and Nafion[®] N211 under saturated inlet gasses at 80 $^{\circ}\text{C}$ and different oxidants can be seen in Figure 4a. The performance of both PolyHPA-75 and PolyHPA-70 are very similar to the performance of Nafion[®] N211, with the PolyHPA-75 fuel cell out performing Nafion[®] N211 at higher current densities.

Using a very simple fuel cell model, this data was fit to further analyse the contributions to the overpotential losses by kinetic, ohmic, and transport factors.^{63,64} The equation used to for the model was:

$$V(i) = E_{ocv} - b \log\left(\frac{i}{i_0}\right) - iR_{hf} + a \log\left(1 - \frac{i}{i_{lim}}\right) \quad [1]$$

where $V(i)$ is the voltage as a function of i (current), E_{ocv} is the open circuit voltage, a and b are fitting parameters and i_0 , R_{hf} , and i_{lim} are the exchange current density, HFR, and limiting current density, respectively. The kinetic, ohmic, and transport losses are the second, third, and fourth terms on the right hand side of equation 1, respectively. The ohmic losses can be seen in Figure 4b. For PolyHPA-75, a 22 % reduction in HFR at 2 A cm^{-2} results in less ohmic losses than PolyHPA-70, which has

nearly the same ohmic losses as the optimized Nafion[®] N211 cell. This is remarkable considering that the PolyHPA-70 fuel cell is 48 μm compared to the thinner Nafion[®] N211 which is 25 μm . The kinetic losses (see Figure 4c) are slightly better for the optimized Nafion[®] N211 fuel cell made with a CCM than for the PolyHPA fuel cells fabricated using commercial GDEs. The last source of losses considered in this model is derived from transport losses (see Figure 4d) and is the cause of poor fuel cell performance in air. To fully take advantage of the PolyHPA, the membrane / electrode interface needs to be optimized and the transport losses in air need to be minimized. Next, the PolyHPA-70 fuel cell was evaluated under low humidity operation at 80 $^{\circ}\text{C}$, see Figure 5. A drop in voltage and an increase in HFR is seen, as expected. At low current densities the HFR starts out near 1000 $\text{m}\Omega \text{cm}^2$, but drops to 141 $\text{m}\Omega \text{cm}^2$ at 2 A cm^{-2} .



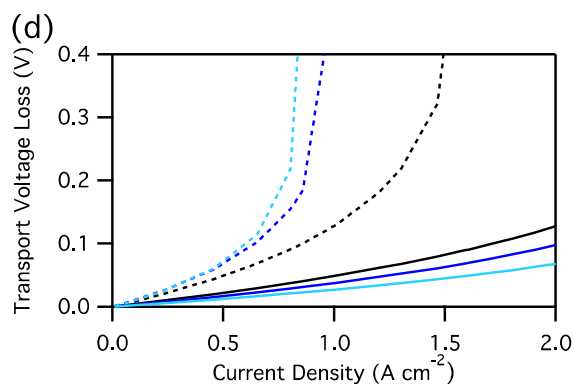


Figure 4: (a) I-V data for Nafion® N211 (25 μm), PolyHPA-70 (48 μm), and PolyHPA-75 (20 μm) at 80 $^{\circ}\text{C}$ and saturated inlet gases with both air (O) and O_2 (X). Experimental data are markers and simulated data is the line, as indicated in the legend. The simulated ohmic (b), kinetic (c), and transport (d) voltage losses vs. current density.

This HFR drop can be attributed to increase in water generation from increasing current densities. Looking at the HFR values at low current density, an order of magnitude increase occurs when the humidity is reduced from 100 to 50 %RH, which is in agreement with the *ex-situ* PEIS data at lower humidities, as can be seen in **Error! Reference source not found.**

The transport rate of H_2 in the device are similar to Nafion® N211. The H_2 crossover, normalized for thickness, is slightly higher for PolyHPA-70 ($0.69 \mu\text{mol cm}^{-2} \text{h}^{-1}$) than for Nafion® N211 ($0.56 \mu\text{mol cm}^{-2} \text{h}^{-1}$) at 80 $^{\circ}\text{C}$. Two routes for improving chemical stability are reducing the crossover of H_2 and adding a radical decomposition catalyst. Due to the similar H_2 crossover values, it can be concluded that the HSiW11 is indeed acting as a radical decomposition catalyst. The H_2O transport rate in PolyHPA-70 is double that of Nafion® N211 (0.55 , and $1.10 \mu\text{mol cm}^{-1} \text{h}^{-1}$, respectively). All of the species transport data (see Figure 6) have been normalized for film thickness to provide a fair comparison.

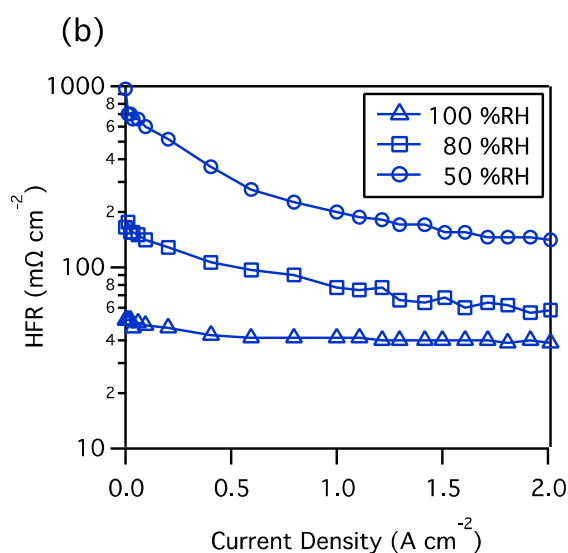


Figure 5: PolyHPA-75 voltage (a) and HFR (b) at different humidities vs. current at 80 $^{\circ}\text{C}$

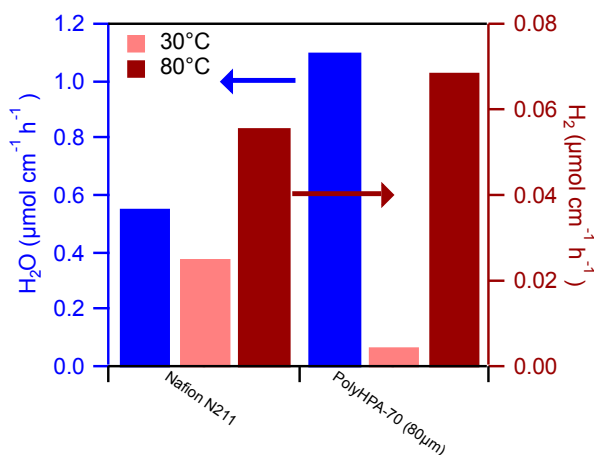
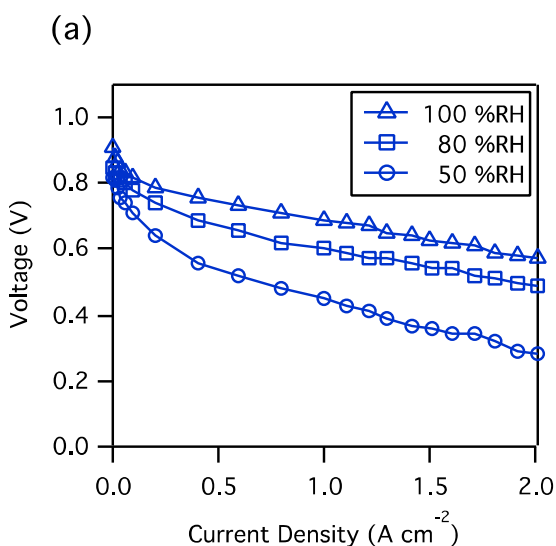


Figure 6: Species transport in MEA for N211, and two different PolyHPA-70 films. The H_2 transport rates were measured at 100 %RH. All values are normalized by thickness



The rapid water transport rate is important, allowing for rapid diffusion of water from the cathode to the anode even with thicker films, which reduces the need for external humidification.

Conclusions

This study has outlined the synthesis of a new material designed to have superior chemical stability and conductivity over PFSA polymer membranes, the current state of the art material. The PolyHPA material is made through attachment of phenol phosphonate ester sidechains to a commercial fluoroelastomer (FC-2178). These sidechains are subsequently converted into the phosphonic acid analogue through a hydrolysis step, yielding PolyPPA. Next, the PolyPPA is reacted with HSiW11 forming covalent bonds, immobilizing the HSiW11.

Both IR and NMR (^1H , ^{19}F , ^{31}P) confirm the synthesis of a new material. SAXS and FIB/TEM indicate that the HSiW11 are clustering, which is hypothesized to be reducing the H^+ transport under low water content due to the non-continuous nature of these clusters. Even so, we have achieved very high proton conductivities of 0.228 and 0.298 S cm^{-1} for the PolyHPA-70 and PolyHPA-75, respectively, when humidified (80 °C and 95 %RH). This material offers a true shift in paradigm on chemical degradation mitigation. All previous strategies have used radical scavenging moieties that are not covalently bound to the polymer backbone and are free to migrate or potentially leach out of the film. In addition to this huge shortcoming of other approaches, most additives do not contribute to proton conductivity and addition of too much will lead to performance losses. Our method overcomes these challenges and resulted in outstanding chemical stability under chemical ASTs with a demonstrated OCV decay rate of 100 $\mu\text{V h}^{-1}$ under a $\text{H}_2\text{-O}_2$ environment. Additionally, the HFR is 22 % lower in our films than in Nafion[®]. Future work is needed to fully understand the relationship between the morphology and proton transport as well as to develop optimized electrodes for this fuel cell system. Additionally, making thin (ca. 10 μm) composite films with mechanical support would further improve fuel cell performance. Incorporation of different HPA moieties into this polymer system is also being investigated. This initial study highlights the potential for this PolyHPA platform to be integrated into a durable, high performance fuel cell.

Conflicts of interest

There are no conflicts to declare

Acknowledgements

The authors would like to thank the U.S. Department of Energy for funding this work through EERE under contract number DE-EE0006363, Dr. Guido Bender from the National Renewable Energy Lab for helping with mechanical testing, and Dr. Matt Frey and Ms. Hui Ren from the 3M Company for preliminary work on this project. This research used resources of the Advanced Photon Source, a U.S. Department of Energy (DOE) Office of Science User Facility operated for the DOE Office of Science by Argonne National Laboratory under Contract No. DE-AC02-06CH11357.

Notes and References

1. T. E. Springer, Zawodzinski, T. A., Gottesfeld, S., *Journal of The Electrochemical Society*, 1991, **138**, 2334-2342.
2. M. Klingele, M. Breitwieser, R. Zengerle and S. Thiele, *J. Mater. Chem. A*, 2015, **3**, 11239-11245.
3. A. Kongkanand and M. F. Mathias, *J Phys Chem Lett*, 2016, **7**, 1127-1137.
4. S. Kundu, M. W. Fowler, L. C. Simon and S. Grot, *Journal of Power Sources*, 2006, **157**, 650-656.

5. R. Borup, J. Meyers, B. Pivovar, Y. S. Kim, R. Mukundan, N. Garland, D. Myers, M. Wilson, F. Garzon, D. Wood, P. Zelenay, K. More, K. Stroh, T. Zawodzinski, J. Boncella, J. E. McGrath, M. Inaba, K. Miyatake, M. Hori, K. Ota, Z. Ogumi, S. Miyata, A. Nishikata, Z. Siroma, Y. Uchimoto, K. Yasuda, K. Kimijima and N. Iwashita, *Chem Rev*, 2007, **107**, 3904-3951.
6. A. Kusoglu and A. Z. Weber, *J Phys Chem Lett*, 2015, **6**, 4547-4552.
7. A. Kusoglu and A. Z. Weber, *Chem Rev*, 2017, **117**, 987-1104.
8. Y. Tang, A. Kusoglu, A. M. Karlsson, M. H. Santare, S. Cleghorn and W. B. Johnson, *Journal of Power Sources*, 2008, **175**, 817-825.
9. M. Zatoń, J. Rozière and D. J. Jones, *Sustainable Energy Fuels*, 2017, **1**, 409-438.
10. S. Y. Lee, D. W. Shin, C. Wang, K. H. Lee, M. D. Guiver and Y. M. Lee, *Electrochemistry Communications*, 2013, **31**, 120-124.
11. Z. Shi and S. Holdcroft, *Macromolecules*, 2005, **38**, 4193-4201.
12. S. Y. Lee, N. R. Kang, D. W. Shin, C. H. Lee, K.-S. Lee, M. D. Guiver, N. Li and Y. M. Lee, *Energy & Environmental Science*, 2012, **5**, 9795-9802.
13. N. Li, S. Y. Lee, Y.-L. Liu, Y. M. Lee and M. D. Guiver, *Energy Environ. Sci.*, 2012, **5**, 5346-5355.
14. C. H. Park, S. Y. Lee, D. S. Hwang, D. W. Shin, D. H. Cho, K. H. Lee, T. W. Kim, T. W. Kim, M. Lee, D. S. Kim, C. M. Doherty, A. W. Thornton, A. J. Hill, M. D. Guiver and Y. M. Lee, *Nature*, 2016, **532**, 480-483.
15. D. E. Curtin, R. D. Lousenberg, T. J. Henry, P. C. Tangeman and M. E. Tisack, *Journal of Power Sources*, 2004, **131**, 41-48.
16. C. S. Gittleman, F. D. Coms and Y.-H. Lai, 2012, DOI: 10.1016/b978-0-12-386936-4.10002-8, 15-88.
17. L. Gubler and W. H. Koppenol, *Journal of The Electrochemical Society*, 2012, **159**, B211-B218.
18. P. Trogadas, J. Parrondo and V. Ramani, *Electrochemical and Solid-State Letters*, 2008, **11**, B113-B116.
19. D. Banham, S. Ye, S. Knights, S. M. Stewart, M. Wilson and F. Garzon, *Journal of Power Sources*, 2015, **281**, 238-242.
20. A. M. Baker, R. Mukundan, D. Spornjak, E. J. Judge, S. G. Advani, A. K. Prasad and R. L. Borup, *Journal of The Electrochemical Society*, 2016, **163**, F1023-F1031.
21. A. M. Baker, S. K. Babu, R. Mukundan, S. G. Advani, A. K. Prasad, D. Spornjak and R. L. Borup, *Journal of The Electrochemical Society*, 2017, **164**, F1272-F1278.
22. Andrew M. Baker, S. T. D. Williams, R. Mukundan, D. Spornjak, S. G. Advani, A. K. Prasad and R. L. Borup, *J. Mater. Chem. A*, 2017, **5**, 15073-15079.
23. A. M. Herring, *Journal of Macromolecular Science, Part C: Polymer Reviews*, 2006, **46**, 245-296.
24. V. Ramani, H. R. Kunz and J. M. Fenton, *Electrochimica Acta*, 2005, **50**, 1181-1187.
25. G. M. Haugen, F. Meng, N. V. Aieta, J. L. Horan, M.-C. Kuo, M. H. Frey, S. J. Hamrock and A. M. Herring, *Electrochemical and Solid-State Letters*, 2007, **10**, B51-B55.
26. R. Paul Brooker, L. J. Bonville and D. K. Slattey, *Journal of the Electrochemical Society*, 2012, **160**, F75-F80.

27. D. C. Duncan, R. C. Chambers, E. Hecht and C. L. Hill, *Journal of the American Chemical Society*, 1995, **117**, 681-691.
28. D. Chen, Z. Xue and Z. Su, *Journal of Molecular Catalysis A: Chemical*, 2004, **208**, 91-95.
29. K. Kamata, K. Yonehara, Y. Sumida, K. Yamaguchi, S. Hikichi and N. Mizuno, *Science*, 2003, **300**, 964-966.
30. S. Rowshanzamir, S. J. Peighambaroust, M. J. Parnian, G. R. Amir Khanlou and A. Rahnavard, *International Journal of Hydrogen Energy*, 2015, **40**, 549-560.
31. B. Zhang, Y. Cao, Z. Li, H. Wu, Y. Yin, L. Cao, X. He and Z. Jiang, *Electrochimica Acta*, 2017, **240**, 186-194.
32. J. L. Malers, M.-A. Sweikart, J. L. Horan, J. A. Turner and A. M. Herring, *Journal of Power Sources*, 2007, **172**, 83-88.
33. S. L. N. H. Rhoden, C. A. Linkous, N. Mohajeri, D. J. Diaz, P. Brooker, D. K. Slattey and J. M. Fenton, *Journal of The Electrochemical Society*, 2010, **157**, B1095.
34. M. M. Hasani-Sadrabadi, E. Dashtimoghadam, F. S. Majedi, H. Moaddel, A. Bertsch and P. Renaud, *Nanoscale*, 2013, **5**, 11710-11717.
35. M. M. Hasani-Sadrabadi, E. Dashtimoghadam, F. S. Majedi, J. J. VanDersarl, A. Bertsch, P. Renaud and K. I. Jacob, *Nano Energy*, 2016, **23**, 114-121.
36. O. Nakamura, T. Kodama, I. Ogino and Y. Miyake, *Chemistry Letters*, 1979, DOI: Doi 10.1246/Cl.1979.17, 17-18.
37. U. Lavrenčič Štangar, B. Orel, J. Vince, V. Jovanovski, H. Spreizer, A. Šurca Vuk and S. Hočevar, *Journal of Solid State Electrochemistry*, 2004, **9**, 106-113.
38. J. L. Horan, A. Genupur, H. Ren, B. J. Sikora, M.-C. Kuo, F. Meng, S. F. Dec, G. M. Haugen, M. A. Yandrasits, S. J. Hamrock, M. H. Frey and A. M. Herring, *ChemSusChem*, 2009, **2**, 193-193.
39. J. L. Horan, A. Lingutla, H. Ren, M. C. Kuo, S. Sachdeva, Y. Yang, S. Seifert, L. F. Greenlee, M. A. Yandrasits, S. J. Hamrock, M. H. Frey and A. M. Herring, *Journal of Physical Chemistry C*, 2014, **118**, 135-144.
40. Y. Liu, J. L. Horan, G. J. Schlichting, B. R. Caire, M. W. Liberatore, S. J. Hamrock, G. M. Haugen, M. A. Yandrasits, S. n. Seifert and A. M. Herring, *Macromolecules*, 2012, **45**, 7495-7503.
41. A. R. Motz, M.-C. Kuo and A. M. Herring, *ECS Transactions*, 2017, **80**, 565-570.
42. A. Taguet, B. Ameduri and B. Boutevin, *Fuel Cells*, 2006, **6**, 331-339.
43. A. Taguet, B. Ameduri and B. Boutevin, *Advances in Polymer Science*, 2005, **184**, 127-211.
44. A. L. Logothetis, *Progress in Polymer Science*, 1989, **14**, 251-296.
45. C. R. Mayer, P. Herson and R. Thouvenot, *Inorganic Chemistry*, 1999, **38**, 6152-6158.
46. G. S. Kim, K. S. Hagen and C. L. Hill, *Inorganic Chemistry*, 1992, **31**, 5316-5324.
47. V. Ramani, H. R. Kunz and J. M. Fenton, *Journal of Membrane Science*, 2004, **232**, 31-44.
48. D.-J. Wang, Z.-D. Fang and X.-H. Wei, *Chinese Journal of Chemistry*, 2005, **23**, 1600-1606.
49. S. Neelakandan, D. Rana, T. Matsuura, A. Muthumeenal, P. Kanagaraj and A. Nagendran, *Solid State Ionics*, 2014, **268**, 35-41.
50. M. J. Janik, B. B. Bardin, R. J. Davis and M. Neurock, *J Phys Chem B*, 2006, **110**, 4170-4178.
51. D. Jouannet, T.-N. Pham, S. Pimbert and G. Levesque, *Polymer*, 1997, **38**, 5137-5147.
52. M. Cappadonia, *Solid State Ionics*, 1995, **77**, 65-69.
53. J. S. Pedersen, *Advances in Colloid and Interface Science*, 1997, **70**, 171-210.
54. G. R. Strobl, *The Physics of Polymers: Concepts for Understanding Their Structures and Behavior*.
55. G. R. Strobl and M. Schneider, *Journal of Polymer Science: Polymer Physics Edition*, 1980, **18**, 1343-1359.
56. P. J. James, J. A. Elliott, T. J. McMaster, J. M. Newton, A. M. S. Elliott, S. Hanna and M. J. Miles, *Journal of Materials Science*, 2000, **35**, 5111-5119.
57. M. Inaba, T. Kinumoto, M. Kiriake, R. Umebayashi, A. Tasaka and Z. Ogumi, *Electrochimica Acta*, 2006, **51**, 5746-5753.
58. X. Huang, R. Solasi, Y. Zou, M. Feshler, K. Reifsnider, D. Condit, S. Burlatsky and T. Madden, *Journal of Polymer Science Part B: Polymer Physics*, 2006, **44**, 2346-2357.
59. Y.-H. Lai, C. K. Mittelsteadt, C. S. Gittleman and D. A. Dillard, *Journal of Fuel Cell Science and Technology*, 2009, **6**, 021002.
60. A. Ohma, S. Suga, S. Yamamoto and K. Shinohara, *Journal of The Electrochemical Society*, 2007, **154**, B757.
61. A. Ohma, S. Yamamoto and K. Shinohara, *Journal of Power Sources*, 2008, **182**, 39-47.
62. R. Yadav, G. DiLeo, N. Dale and K. Adjemian, *ECS Transactions*, 2013, **53**, 187-199.
63. A. Z. Weber, R. L. Borup, R. M. Darling, P. K. Das, T. J. Dursch, W. Gu, D. Harvey, A. Kusoglu, S. Litster, M. M. Mench, R. Mukundan, J. P. Owejan, J. G. Pharoah, M. Secanell and I. V. Zenyuk, *Journal of the Electrochemical Society*, 2014, **161**, F1254-F1299.
64. L. M. Pant, Z. Yang, M. L. Perry and A. Z. Weber, *Journal of The Electrochemical Society*, 2018, **165**, F3007-F3014.
65. H. W. Starkweather, R. C. Ferguson, D. B. Chase and J. M. Minor, *Macromolecules*, 1985, **18**, 1684-1686.
66. C. Rocchiccioli-Deltcheff, M. Fournier, R. Franck and R. Thouvenot, *Inorganic Chemistry*, 1983, **22**, 207-216.
67. W. Förner and H. M. Badawi, *Journal of Structural Chemistry*, 2011, **52**, 471-479.
68. A. Taguet, B. Ameduri and B. Boutevin, *Journal of Polymer Science Part a-Polymer Chemistry*, 2006, **44**, 1855-1868.
69. S. Kobayashi, T. Chow, H. Kawabata and T. Saegusa, *Polymer Bulletin*, 1986, **16**, 269-276.
70. K. Y. Matsumoto and Y. Sasaki, *Bulletin of the Chemical Society of Japan*, 1976, **49**, 156-158.
71. J.-Y. Niu, J.-W. Zhao and J.-P. Wang, *Inorganic Chemistry Communications*, 2004, **7**, 876-879.